

## Chapter 3

# Effects of localised shearing on crystal growth and nucleation

As outlined in Chapter 1, the original outline of the project is to investigate the possibility of using optical tweezing to induce nucleation by generating fluid flow within a supersaturated solution. The intent of which would be twofold: Firstly to have a repeatable means of inducing nucleation under different solution conditions. And secondly, to understand the influence of shearing on nucleation at a micro level as compared to results in bulk fluid. It has been shown that for macro-scale systems, the likelihood of nucleation increases to a maximum value under increased shearing [5, 16]. Mura and Zaccone developed a theoretical framework to describe how the a newly formed nucleus experiences two additional growth factors when placed in a moving fluid. Firstly, due to increased molecular transport of solute molecules the nucleation rate is enhanced in low to moderate fluid flows. But in addition, due to shear flow the crystal surface undergoes deformation which suppresses the nucleation rate undergoing faster fluid flow [16]. The theory was confirmed for glycine solution by Debuyschere *et al* who identified that the nucleation rate of supersaturated glycine was enhanced up until  $\dot{\gamma} \approx 3000 \text{ s}^{-1}$  [5]. After which the nucleation rate began to decrease but was still greater compared to the case where fluid flow was minimal.

Optical tweezers can been used to rotate a whole host of micro-rotors, with the

fastest reported results exceeding 1000  $Hz$  in heavy water [1]. Therefore, it stands to reason that a micro-rotor rotating in a supersaturated solution could generate sufficient fluid flow such that the nucleation rate around said particle is enhanced compared to the bulk fluid. We focused on two primary candidates for micro-rotors, Vaterite and 4-Heptyl-4-biphenylcarbonitrile (7CB). The former being a polymorph of calcium carbonate and the latter an example of nematic liquid crystals, both of which have been used repeatedly in previous micro-rotor. In addition, we also consider the application of using techniques beam steering to generate fluid flow by trapping silica micro-beads. In this instance the fluid flow is generated not due to the transfer of angular momentum, but due to shearing caused by a moving sphere through stagnant fluid.

To begin with, the discussion of the necessary optical equipment is covered, drawing attention to specialised components and techniques that are not standard in optical trapping set ups.

### 3.1 Optical Tweezer Equipment

In general, all optical tweezers require a laser driver, a focusing microscope objectives, a position controller, and position detector. The laser used for this project was a  $1064\text{ nm}$  near infrared laser - provided by CNI Lasers – that was focused by a Nikon 100x oil immersion lens. The choice of an oil immersion lens is important as the optical oil used prevents a loss of focus when used on a glass cover slip. Now, experimental work has shown that the trapping efficiency increases with beam diameter up until it exceeds  $\frac{2}{3}D_{obj}$  [11] where  $D_{obj}$  is the diameter of the objective aperture. To expand the beam front we utilise a Galilean beam expansion arrangement (indicated by  $f_1$ , and  $f_2$  in Fig. 3.1) as recommended for high power laser applications. In our initial experiments the beam expansion provides a  $4\times$  magnification. Whereas in later experiments we utilised a galvano-mirror the beam expansion is  $3\times$  and then the 4f correlator provides a further  $1.25\times$  magnification (using  $f_3$  and  $f_4$ ) - the magnification is given by.

$$\frac{D_2}{D_1} = \frac{f_2}{f_1} \quad (3.1)$$

It should be noted that the galvano-mirror requires the use of a Keplerian beam expansion arrangement which reduces the transmitted laser power due to localised heating of the air. Afterwards the laser is passed through a dichroic mirror that separates incoming infrared and visible light, this is to prevent the laser from damaging the CCD camera used for imaging the trapping plane. The laser is then focused to a diffraction limited spot by the objective. Utilizing a high numerical aperture objective enhances the gradient force at the focal point; the trade-off being that for higher NA objectives the trapping depth is reduced due to spherical aberrations. While it is possible to increase the trapping depth [18] by adjusting the objective's tube length this approach is incompatible with our trapping arrangement. A 0.25 NA condenser objective refocuses the scattered laser light and also provide an aperture for an imaging LED to illuminate the focal plane. Samples are loaded onto a piezo driven table to that is inserted between the trapping and condensing objectives; the piezo drivers allow for sub-micron control of the beam focus position to a degree as small as a 10 nm. To detect and monitor the position of a trapped particle a quadrant photo diode (QPD) was utilised.

### 3.1.1 Position detection methods

In order to accurately capture the dynamics of a trapped particle, a position detection system is required. There are 3 possible methods of position detection: video-analysis, lateral-effect position sensing, and photodiodes. The former being ideally suited for multiple traps or situations where precision is not the top priority. In order to match the force measurements of back-focal plane interferometry requires the camera's frame rate to exceed 1  $kH\bar{z}$  which can be difficult to achieve while maintaining a decent resolution [9]. In comparison off the shelf back-focal plane detectors can achieve temporal resolutions anywhere from 10 – 100  $kH\bar{z}$  [2].

A quadrant photo diode (QPD) is a frequently used position detection system for optical tweezers due to their high sampling rate, high degree of precision, and ease of set up. The QPD is constructed of four photo diodes assembled in a quadrant formation, when a particle is trapped the interference pattern produced is focused onto the QPD, with the maximum intensity mapping to the particle's centre of mass. By summing

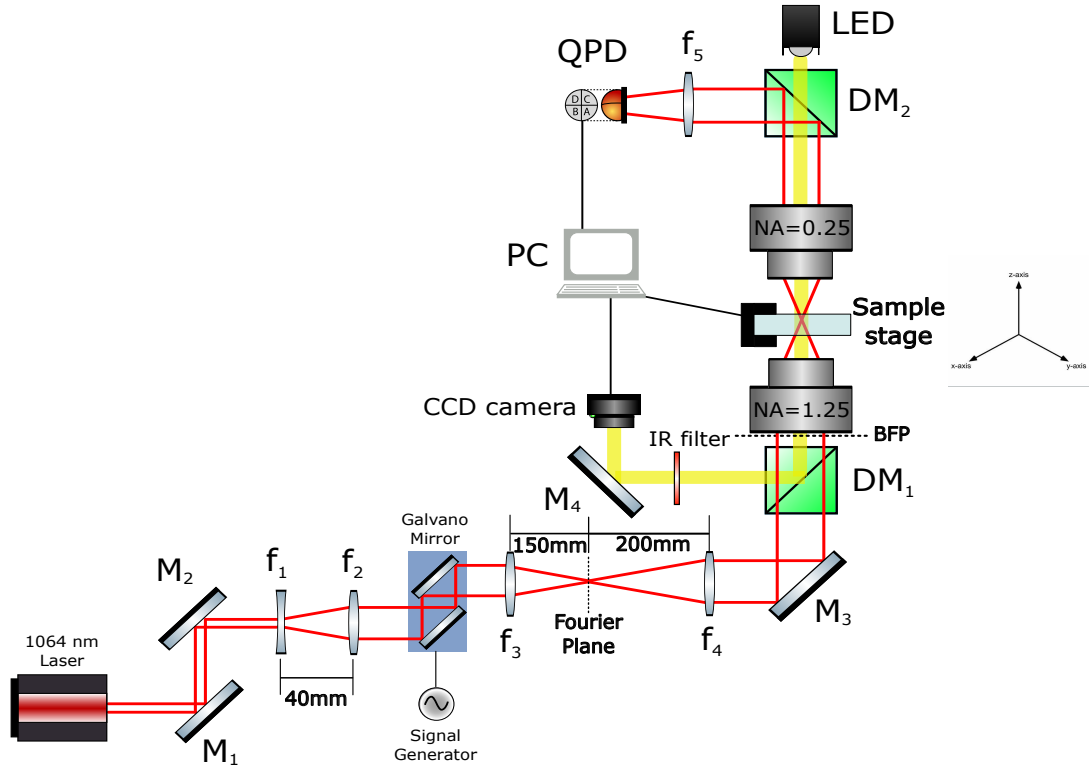


Figure 3.1: Optical tweezer set up used for the majority of the PhD. The focal lengths of  $f_1$ ,  $f_2$ ,  $f_3$ , &  $f_4$  are  $-20\text{ mm}$ ,  $60\text{ mm}$ ,  $150\text{ mm}$ , &  $200\text{ mm}$  respectively. Diagram not drawn to scale.

the voltages of the horizontal and vertical quadrants together the particle's centre of mass is tracked in the x-y plane. Axial displacement can be estimated by observing the change in the total voltage of the QPD. The outputted signal gives an indication of the particle's relative displacement from the beam focus, but in order to convert the signal to distance units the trap needs to be calibrated (assuming a linear response curve).

A lateral-effect sensor has a similar output but works using the entire sensor as a single cell analogous to the focal plane of the trapping beam. The four corners of the sensor act as anodes connected to a base plate cathode, as the beam moves across the surface of the detector each anode will experience a different photocurrent depending on how close the centre of the interference pattern is to each anode. The advantage of a lateral effect detector is that the linear regime is much larger than a QPD making it much better for monitoring the position of a trapped particle. However, Lateral-effect

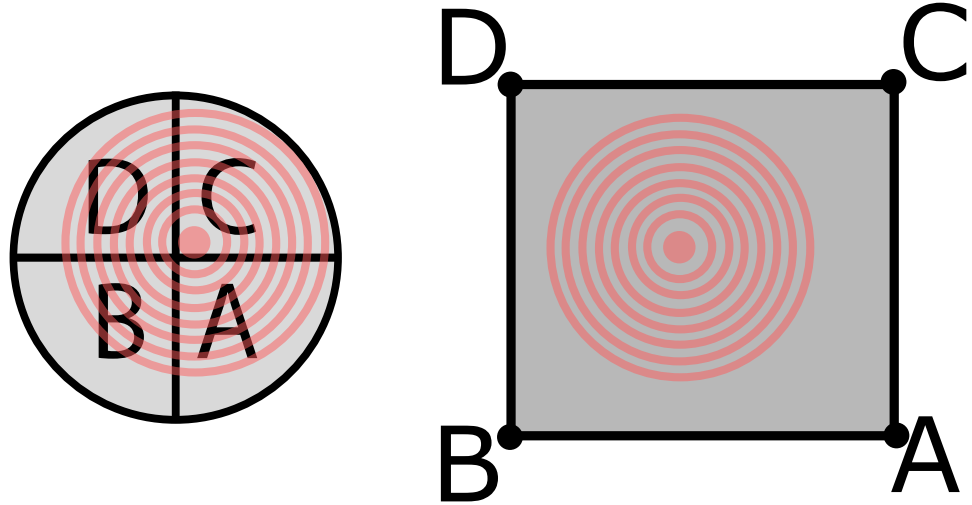


Figure 3.2: Comparison between QPD and Lateral effect photodiodes. The four quadrants of a QPD (left) experience different photocurrents based on the total intensity of light incident on each section (labelled A, B, C, D). Whereas a Lateral effect sensor (right) uses the resistive properties of the photodiode surface to vary the create different photocurrents passing through the anodes A, B, C, and D.

sensors are often limited in their spacial resolution due to high signal-to-noise ratios, requiring a high intensity of light on the sensor in order to get a clean signal. As a result, most optical force measurements are conducted using a QPD as opposed to a lateral-effect sensor, as often the displacement is small enough that the signal-displacement curve can be considered linear.

### 3.1.2 Fourier Optics and 4f correlators

A 4f correlator is an example of Fourier optics in practice, understanding that a focused lens takes a Fourier transform of the light profile. Consider a laser with a circular Gaussian profile, if you were to place a detector there you would pick up the intensity as a function of its position within the beam. If however you focused the light into

### Chapter 3. Effects of localised shearing on crystal growth and nucleation

a single point (using a +ve focal lens) you are actually seeing a measurement of the phase of your laser with position, in which you would see a diffraction limited spot ( $d = \lambda/2n\sin(\theta)$ ), indicating that the laser is collimated. In imaging systems, a series of focal lenses can be used to filter out unwanted scattering from an image (or in an inverse case differentiate between different images), the placement of each lens is shown below.

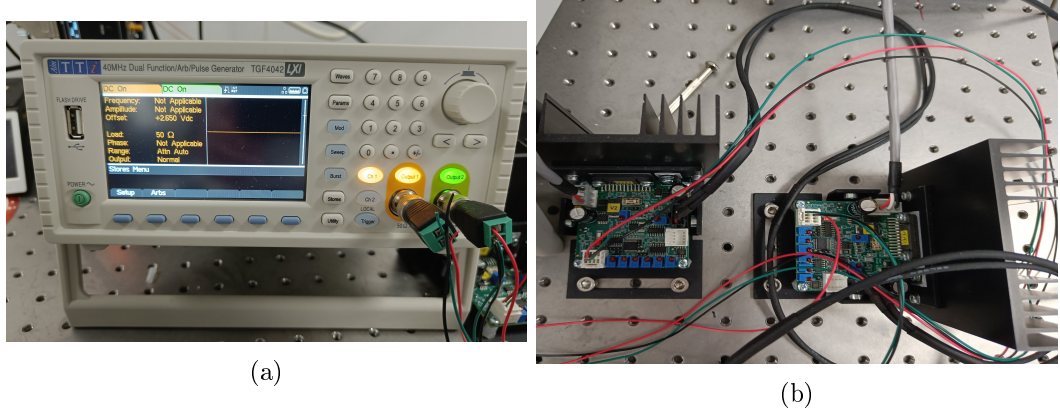


Figure 3.3: Signal generator galvano mirror controller, channel 1 controls the x-axis mirror, while channel 2 controls the y-axis mirror. Both channels can be manipulated independently.

For our applications a 4f correlator is utilised to ensure that the motion of the galvano-mirrors does not move the focal point of the laser, allowing for a stable trap even while in motion. As shown in Fig. 3.1, after the galvano-mirror we have our two lenses -  $f_3$  and  $f_4$  - the former being installed 150 mm from the second mirror of the galvano, and the latter being installed 200 mm from the back focal plane of the trapping objective. The signal generator used was supplied by 'MCS Test Equipment Ltd', allowing for dual channel signal control. This allowed us to precisely control the alignment, amplitude, phase, and frequency of both mirrors making alignment much easier. For basic trapping calibration the galvano-mirrors were set to a simple DC output, providing a fixed spot which operates like a typical optical trap.

## 3.2 Synthesis of Birefringent Micro spheres

There are several options for particles that can be rotated using optical tweezers [17,22]. Over the course of the project two different micro spheres where investigated, Vaterite and liquid crystal droplets. Both can be readily synthesised in the lab and are will rotate at a variety of sizes.

Vaterite is a polymorph of calcium carbonate that is rarely seen in nature due to its low stability [13]. However unlike its other polymorphs of calcite and aragonite, when synthesised Vaterite will typically form small spherical particles making them ideal for optical trapping and rotation. Synthesis of Vaterite micro spheres requires fine control of the crystal growth process in order to maintain polymorphic stability. Though for the purposes of optical rotation the exact polymorph is not as important as its morphology as all 3 polymorphs are inherently birefringent.

Vaterite samples where made by the first preparing equal amounts of  $CaCl_2$  and  $Na_2CO_3$  at a concentration of  $0.33M$ , at the same time a vial of  $0.33M$   $MgSO_4$  was prepared and set aside for later. First a small vial was filled with  $1.5mL$  of  $CaCl_2$  followed by  $60\mu L$  and  $90\mu L$  of  $MgSO_4$  and  $NaCO_3$  respectively, forming a seed solution. Next, a larger vial was filled with  $5\text{ mL}$ ,  $1.5\text{ mL}$ , and  $1\text{ mL}$  of  $CaCL_2$ ,  $MgSO_4$ , and  $NaCO_3$  respectively followed by the seed solution. After 10 minutes of slow but continuous mixing a few drops of Agepon was added to halt the reaction, the solution was filtered and washed 3 times with distilled water before being suspended in water.

When trapped in circularly polarised light, the anisotropic crystal lattice allows spin angular momentum to be transferred to the Vaterite particle, resulting in a rotation about the beam axis. In addition, the anisotropic scattering causes the QPD signal to vary with a constant periodicity that is attributed to its rotation rate. Therefore, the resulting power spectrum is not a Lorentzian but now also displays peaks that appear at integer multiples of the particles rotational frequency.

As shown by Fig. 3.4(b) the power spectra produced still demonstrates a Lorentzian curve but modified with these periodic peaks, while the Lorentzian can be loosely fitted to the end tail there exists no current model for describing the power spectra. The

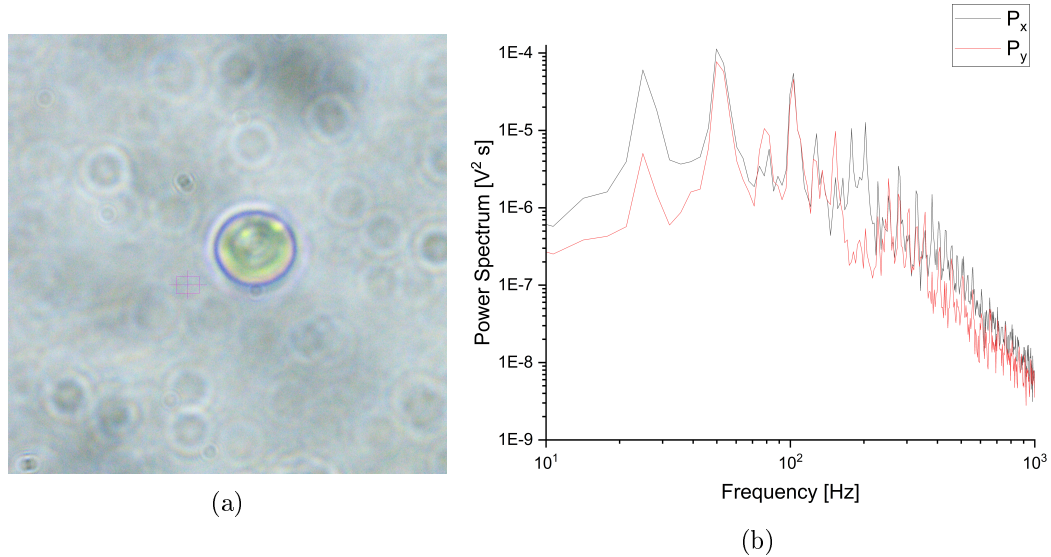


Figure 3.4: (a) Sample Vaterite sphere suspended in water and trapped by circular polarised trap. (b) Collected power spectrum from rotating Vaterite, peaks in the power spectrum appear at integer multiples of the rotational frequency ( $f_{rot} \approx 49.8$  Hz)

closest approximation to this was conducted by [28] where they describe the rotational motion of ellipsoidal polystyrene particles. The critical assumption being that the particle perfectly rotates in the  $x - y$  plane. It has long been suspected that birefringent microspheres experience torques outside of the  $x - y$  plane [26] making it very difficult to characterise the behaviour of rotating birefringent microspheres without a proper understanding of the full optical torque being applied to it.

### 3.2.1 Liquid Crystal Rotors

Liquid crystals are an intriguing example of materials with mixed phase properties. Unlike typical solutes such as Glycine, a liquid crystal can still maintain some degree of order between its individual molecules while in the liquid state. This is due to the fact that liquid crystals are constructed of ordered molecules that demonstrate a long range ordering. There are three main types of liquid crystal transition methods: Thermotropic crystals will transition to their liquid crystal phase when sufficiently heated. Lyotropic materials can undergo this transition due to changes in temperature and concentration. And lastly, Metallotropic materials - which are composed of both organic

and inorganic molecules - change phase according to the ratio of organic to inorganic molecules present. Liquid crystal rotors are rather simple in their production, 4-Heptyl-4-biphenylcarbonitrile (7CB) was purchased from Sigma Aldrich and a small amount was added to a vial of distilled water. The solution was then heated in a water bath to 25° in order to transition the solid crystal into its liquid crystal state. The solution can then be loaded onto a sample cover slip and the individual droplets visualised. The molecules of 7CB will align with a strong electric field, and due to the spherical droplet geometry the droplets are inherently birefringent.

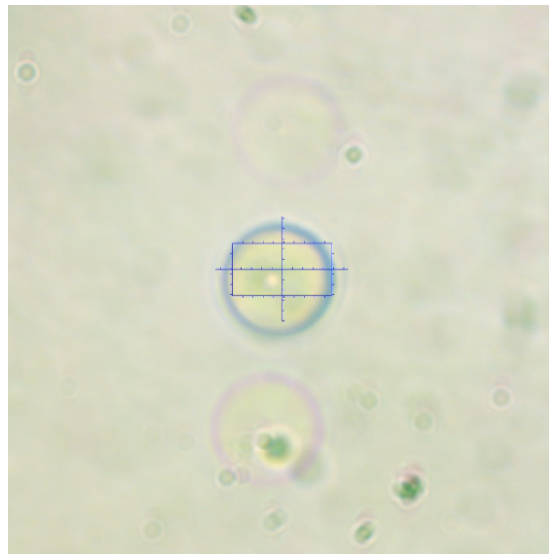


Figure 3.5: Liquid crystal undergoing rotation due to the circularly polarised trap.

The liquid crystal droplets had a much faster rotation rate than comparable Vaterite spheres, due to their higher degree of birefringence and the fact that the droplets are far closer to perfect spheres making angular momentum transfer more efficient.

### 3.3 Rotation of birefringent micro spheres

Optical tweezing has often been used for micro-rheology, by computing the exact forces being exerted on the trapped sphere, one can determine the local temperature/viscosity of the medium [15, 20]. Using a birefringent particle and rotating it within the fluid, the maximum rotation rate is due to the fluid drag resisting the torque of the trapping

beam [20]. If you want to measure fluid flow you can instead use a micro-rotor to see how fluid flow propagates in the medium [12]. Likewise, one can use a beam steering arrangement to probe the drag force of the fluid, by understanding the trap strength (calibrating using a low frequency signal) one can measure the drag force experienced by the local fluid [19]. I

Understanding the fluid velocity around our trapped object is determined mostly by the Reynold's number of the system, for a sphere submersed in a moving fluid of velocity  $U$  this is given by:

$$Re = \frac{\rho U D}{\mu} \quad (3.2)$$

Where  $D$  is the sphere's diameter, and  $\rho$  and  $\mu$  are the fluid's density and viscosity respectively. In our case we do not have a fluid moving around a sphere but a sphere moving through the fluid at some velocity  $U$ , assuming a no-slip boundary condition we can model the fluid velocity profile based on the velocity of the particle. There are two possible avenues for generating shear flow with a trapped particle; rotation of birefringent particles, and fluid flow induced by particle motion.

Rotating birefringent particles are by far the most common method for generating and measuring fluid flow in a solution. To see if we can even achieve the theoretical maximum shear rate, Vaterite spheres were synthesised (see Sec.3.2) submerged in water and trapped with the 1064 nm laser at set to 450 mW. The rotation frequency was determined using the QPD, and the particle sizes were computed by image analysis. With the particle size and rotation frequency, the tangential rotation speed is calculated via:

$$u(r) = \frac{\pi d^3}{4 r^2} \omega \quad (3.3)$$

Where  $d$  is the particle diameter,  $\omega$  is the rotation frequency reported by the QPD, and  $r$  is the distance from the particle's centre. Using Eq.3.3 we calculated the fluid flow radiating outward from the centre of the sphere. The shear rate can then be computed as the partial derivative fluid flow (assuming shearing is generated purely by the flow

field):

$$\dot{\gamma}(r) = \left| \frac{\delta u(r)}{\delta r} \right| = \frac{\pi}{2} \frac{d^3}{r^3} \omega \quad (3.4)$$

### 3.3.1 Estimation of fluid flow around micro-rotors in bulk fluid

First we determined the upper rotation rate that could be achieved using both Vaterite and liquid crystal spheres. Vaterite samples were synthesised according to [3, 17] (see sec. 3.2), and then suspended in distilled water. A sample of  $200 \mu L$  was pipetted and a single microsphere was captured via a circular polarised beam.

Due to Van der Waal's forces some of the microspheres were stuck together, fortunately individual sphere's were still present. Multiple microspheres were trapped and their rotation rate was determined by looking at the peak frequency component of the collected power spectrum. The shear flow was estimated using eq.(3.4) assuming the spheres were operating in the bulk fluid and away from any boundaries.

From Fig.3.6 there is not a strong relationship between particle size and rotation rate, this is contrary to much of the theoretical predictions that predict an exponential decay with particle size. This can be in part due to the fact that synthesising perfectly spherical spheres that have uniform birefringence across the whole population is difficult. Despite our best efforts at controlling the growth rate the smallest particle ever synthesised was around  $3 \mu m$  in diameter. The Vaterite spheres would often stick together while suspended in water after a short period of time. The fastest reported rotation rate found during this project was by [1] that achieved a rotation rate of  $5 kHz$ , this is plotted on Fig 3.6 as the dotted line. Even at that extreme a rotation rate the region in which nucleation is at its optimal likelihood is only  $20 nm$  wide. If instead the micro-rotor was within the vicinity of a solid boundary, the shear rate would be enhanced due to the no-slip boundary condition.

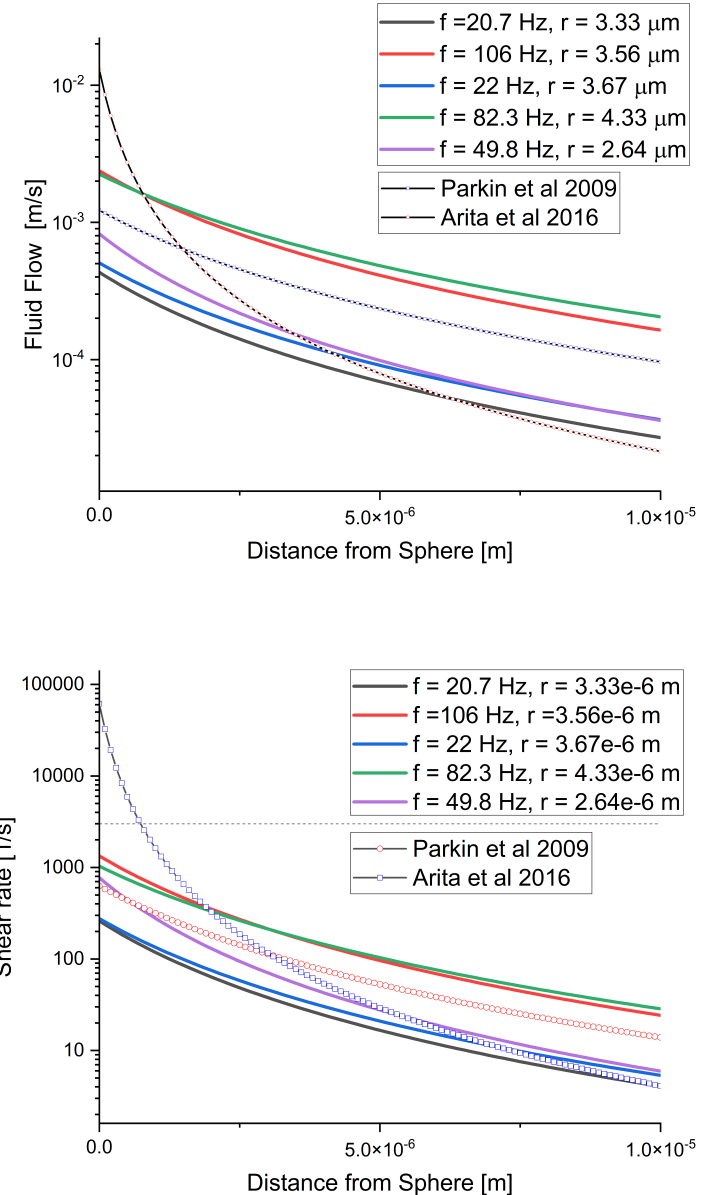


Figure 3.6: (Top) Fluid flow radiating out from the surface of a rotating Vaterite sphere. (Bottom) Shear rates computed using Eq.3.4, optimal shear rate is of  $3000 \text{ s}^{-1}$  is indicated by the dotted line. Vaterite radii and rotation frequencies are shown, the laser power was kept constant at 450 mW. Reported rotation rates, and their corresponding fluid flow and shear rates, for Vaterite are also plotted alongside lab results. Results from [1, 17] are included as well.

### 3.4 Micro-rotors in Supersaturated solution

If rotation rates in bulk solution are insufficient then a micro-rotor rotating close to an artificial barrier may be able to improve the shear rate of the surrounding fluid. Of course placing a solid barrier in a supersaturated fluid may well encourage nucleation somewhere on the surface outside of our control. Instead we chose to use the droplet edge of the supersaturated solution, while not a hard barrier per say, the molecular mobility close to the droplet edge is reduced due to surface tension. Furthermore, it has been shown through multiple results that nucleation is enhanced at the air-solution interface [14, 23, 30].

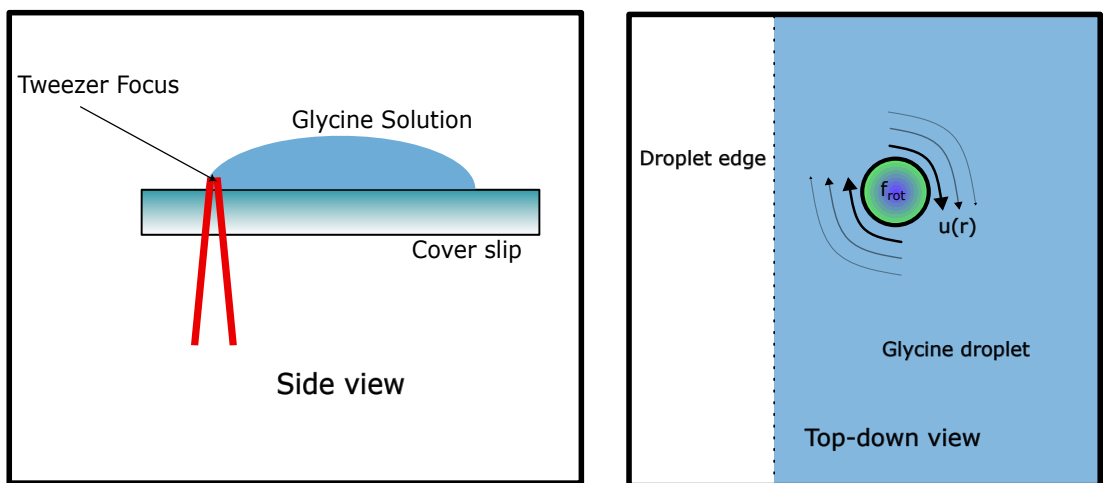


Figure 3.7: Diagram of optical trapping set up for rotating birefringent particles in a supersaturated solution. Left: side view of the trapping set up showing the location of the trap focus at the edge of the droplet of a supersaturated solution. Right: top down view of the glycine droplet with a trapped birefringent particle shown close to edge of the trap. As the particle rotates the drag force from the surrounding fluid generates a flow field around itself (see Eq. 3.3).

Supersaturated solutions of glycine and water were prepared and stored in an incubator prior to use. When ready to be studied 15  $\mu\text{L}$  was pipetted into the solution and 20  $\mu\text{L}$  was pipetted onto the cover slip. A Vaterite sphere was located, trapped, and moved as close to the droplet edge as possible. After measuring the microsphere's rotational frequency the sphere was left to rotate for a period of ten minutes after which, if no nucleation event was observed the particle was released. The overall results are

catalogued in table 3.1

Table 3.1: Results from rotating Vaterite within supersaturated solution of  $H_2O$  and Glycine. Solubility concentration for Glycine at  $16^\circ$  was  $C^* = 0.2016g/g$

Super Saturation	Particle radius [ $\mu$ ]	$\omega$ [Hz]	Nucleation [✓/✗]
1.01	2.34	20.7	✗
	5.67	23.3	✗
	3.26	15.4	✗
1.14	1.89	1.23	✗
	3.75	3.54	✗
	4.35	4.86	✗
1.4	3.47	0.00	✗
	1.59	0.00	✗
	6.24	0.00	✗
1.45	6.32	0.00	✗
	3.68	0.00	✗
	5.43	0.00	✗
1.49	4.76	0.00	✗
	7.27	0.00	✗
	1.52	0.00	✗

Trying to trap a particle close to the edge proved more challenging than expected. Unlike in previous reports where the beam is focused at the upper edge of the droplet [14, 24,30], we attempted trapping into the crook of the droplet. It is suspected that trapping is much harder at the interface due to increased surface tension and unpredictable scattering forces. The closest we could trap a microsphere to the droplet edge was in the range of  $5 - 10\mu m$ , at that distance the fluid flow is so low that even the presence of a hard boundary would be insufficient for shearing the fluid. Furthermore, as is evident in Table 3.1, the rotation rate drops off significantly with increased supersaturation, due to higher fluid viscosities. While in theory a sufficiently focused laser could rotate any microsphere to a fast enough to reach the shear rate predicted by [5] the localised intensity would be so large that even using  $D_2O$  would see a significant increase in temperature.

It is not impossible that fluid shearing could be used in the future to localise nucleation; but from these results, using individual micro-rotors is not an appropriate method. Firstly, the area of influence is far too small to see any noticeable increase

in the nucleation rate. And secondly, increased fluid viscosity significantly reduces the limits the maximum rotation rate possible. If multiple micro-rotors could be trapped in close proximity to one another they could create a large region of fluid where nucleation is more likely than the bulk fluid. Micro-rotors have been created that allow for precise control of suspended micro-particles [4] and could potentially be used to generate sufficient shearing. However these could not be used in this project as we lacked the necessary hardware to form multiple gradient traps.

### 3.5 Shearing via Galvano-mirror manipulation

An alternative approach to generating fluid shear is to use a galvano-mirror to rapidly move a trapped particle in a bulk fluid. While typically galvano and gimble mirrors are used to trap multiple particles simultaneously, a single micro sphere can be moved quickly through a fluid along a preset path. The only limitation on the particle's speed being the ratio of the trap stiffness to the drag force. Calculating the shear rate around an individual particle is difficult to do precisely but for low Reynolds numbers we can get an adequate approximation.

For a simple circular path one can estimate the sphere's speed by the radius of its path and the frequency of its orbit  $U = R\omega$ ; however for a more complex path, such as an elliptical orbit the curve needs to be parametrised. One can describe the position parameter of a circular path as such:

$$r(u) = [r\cos(2\pi u), r\sin(2\pi u), 0] \quad (3.5)$$

If we say that  $u$  describes time from some initial point we can say  $u = t\omega$  where omega is the frequency of orbit. Substituting this in and then taking the partial derivative of position gives:

$$v(t) = \frac{dr(t)}{dt} = [-2\pi r\omega \sin(2\pi t\omega), 2\pi r\omega \cos(2\pi t\omega), 0] \quad (3.6)$$

In order to compute  $U$  we simply take the magnitude of our velocity. For low velocities the fluid flow at the sphere's surface can be computed based on its velocity.

$$u_r(r) = -|v(t)|^2 \cos(\theta) \left( 1 - \frac{3R}{2r} + \frac{R^3}{2r^3} \right) \quad (3.7)$$

Where  $\theta$  is the angle from the direction of movement to the point you wish to measure, and  $r$  is the radial distance to that point. Again taking the partial derivative we can get the shear rate for a particle moving through the fluid:

$$\dot{\gamma}(r) = \left| \frac{\delta u_r(r)}{\delta r} \right| = |v(t)|^2 \cos(\theta) \left( \frac{3R}{r^2} - \frac{2R^3}{r^4} \right) \quad (3.8)$$

Moving a silica bead along a circular path can generate significant fluid flow around a larger volume compared to comparable microspheres.

## 3.6 Nucleation with a Stationary and Moving Beam

As mentioned previously, shearing via optical rotation and particle displacement did not result in any localised nucleation events even while in the proximity of the droplet edge. During the experiments with the galvano-mirror, it was found that when no particle was present in the optical trap nucleation events would occur while the beam was close to the edge of the droplet, even though the solution was undersaturated. This has been reported prior [14, 21], but was more interesting is how the beam's motion influenced the growth of the nucleus.

### 3.6.1 Stationary beam

Consider below in Fig. 3.8 the frames taken from a nucleation event in supersaturated glycine solution ( $S = 1.03$ ), the beam is a stationary being  $\approx 3.5\mu m$  from the droplet edge. After a period of roughly 5 minutes a nucleus forms at the trap focus, growing quickly (growth rate was approximated using imageJ to be on the order of

$700 \mu\text{m}^2/\text{min}$ ) from the focal point of the trap until after roughly 6 seconds the crystal escapes. Comparing to previous literature using optical tweezers shows that the growth rate is only loosely connected to the solutions supersaturation. Local conditions play a much larger role in the growth rate than just the concentration [6]. A likely reason that the trap is escaped is due to the fact that crystal is far too large to be held in place and is in fact still growing as the solution is supersaturated. The key take away to remember is that the beam has no real influence over the crystal shape, instead it grows outward from the trap focus.

### 3.6.2 Moving Beam

To test if a rapidly moving silica bead could generate the necessary shear rate for crystal nucleation we wanted to see if a trapped silica bead could be trapped and moved in an aqueous solution.  $20 \mu\text{L}$  of glycine and water ( $S = 1.03$ ) was added to  $10 \mu\text{L}$  of a dilute water-silica mixture making the solution undersaturated ( $S \approx 0.7$ ). However, due to the beam's motion we instead encountered several unexpected results.

Shown below in Fig. 3.9 where we have the laser focus moving in a small elliptical pattern; interestingly. After a few minutes we noted the appearance of several small droplets, these appear too small to be silica beads which have a uniform radius of  $1.57 \mu\text{m}$ . We surmise these could be small clusters of Glycine that had previously been shown to form when the aqueous solutions where irradiated with a focused laser [10, 25]. While no droplets are seen directly entering the focus a nucleus forms close to the droplet edge, unlike in Fig. 3.8 the crystal does not grow out from the focal point evenly. Due to the galvano mirror, the crystal is simultaneously being moved by and growing around the focal point of the trap. Because of this the crystal nucleus lacks a clear morphology at first. Until roughly  $20 \text{ s}$  the crystal reaches a almost prismatic structure, with further irradiation increasing the size.

Interestingly the galvano-mirror allows the trap to impart a slight torque on the crystal, as shown in fig. 3.9(c) and (d), where even though the crystal is not directly in the trap focus it rotates in the  $x - y$  plane and gets trapped again at a corner. The rotation could not be due to fluid flow close to the surface of the crystal as trap

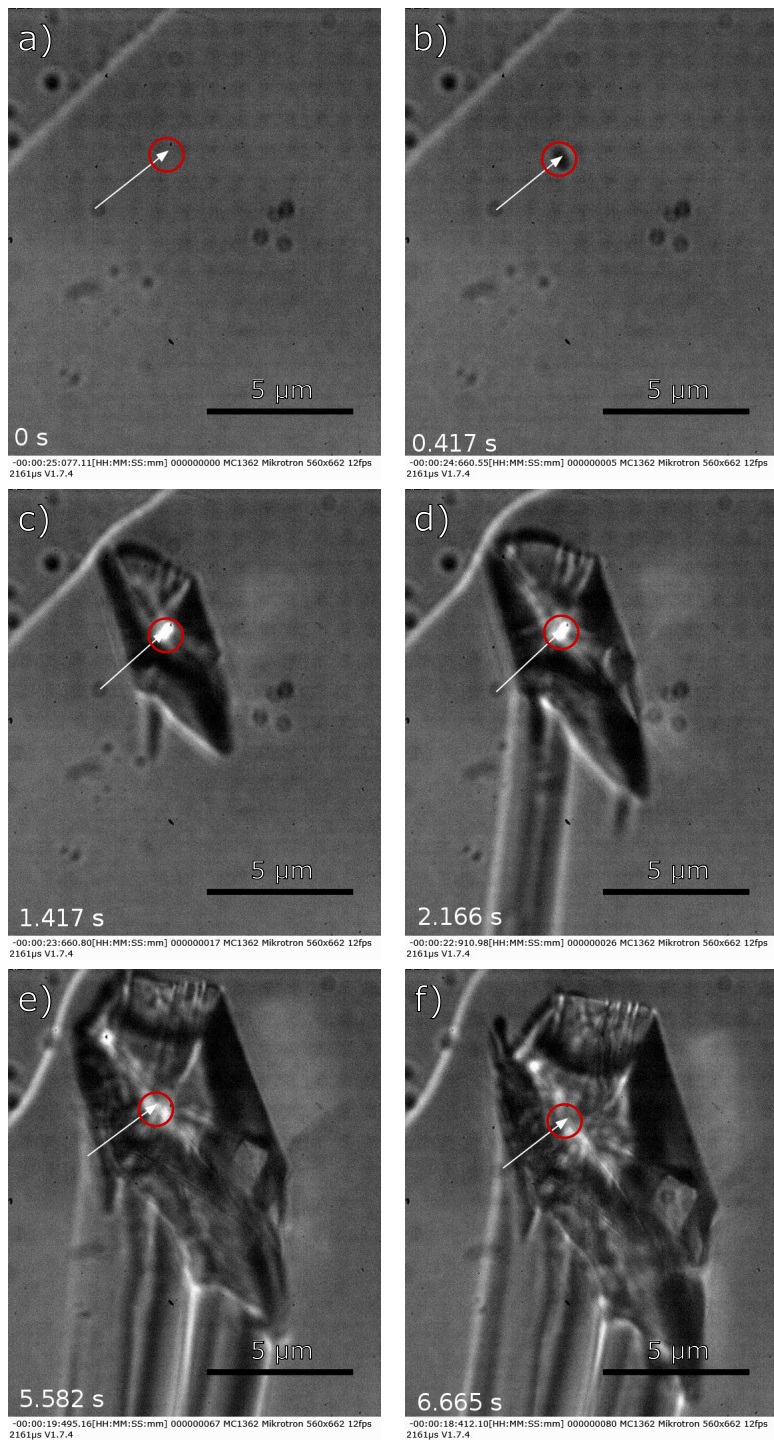


Figure 3.8: Laser induced nucleation at the edge of a droplet of supersaturated glycine solution. (b) shows the first instance of a crystal nucleus, growing quickly through (c)-(e) until after 6.665 s the crystal begins to escape the trap.

should have no influence on fluid molecules smaller than a few hundred nano-meters. In figs.3.9(e) and (f), the crystal growth becomes localised to the corner. The area growth rate between figures 3.9(a) and (d) was approximated using imageJ at  $45.03 \mu\text{m}^2/\text{min}$ , where as between figures 3.9(e) and (f) the growth rate at that particular edge was estimated at  $42.10 \mu\text{m}^2/\text{min}$ .

Nucleation in undersaturated conditions has been reported previously in  $D_2O$  [21] and  $H_2O$  [6]. Though notably in both cases the crystal morphology is not influenced by the location of the laser focus, nor do they report the appearance of glycine droplets. Reports of these droplets has been found only in supersaturated conditions, often using a lower NA objective to provide a wider trap focus [14, 29, 30].

### 3.6.3 Direct trapping of Glycine clusters

One common aspect involving these droplets is the fact when brought to the laser focus the droplets would nucleate immediately [14]. We made up a solution similar to Sec 3.6.2 but without any silica droplets, we once again focused the beam close to the droplet edge. Again after a few minutes of irradiation we noted the presence of droplets, because no silica had been added these droplets had to be from the glycine solution. Trapping these

It has been shown that polarisation can influence the polymorphic control for simple salts [7, 8] but no research has been done into the influence of a moving beam front on the growth of a newly formed nucleus.

## 3.7 Influence of a moving beam front on seed crystals

To see if the above phenomena had any direct influence on a

## 3.8 Summary of Moving Beam Phenomena

To summarise, the introduction of a moving beam helps to accelerate the local growth of a newly formed crystal. This is due to the presence of glycine droplets that accumulate near the interface between the liquid solution and air.

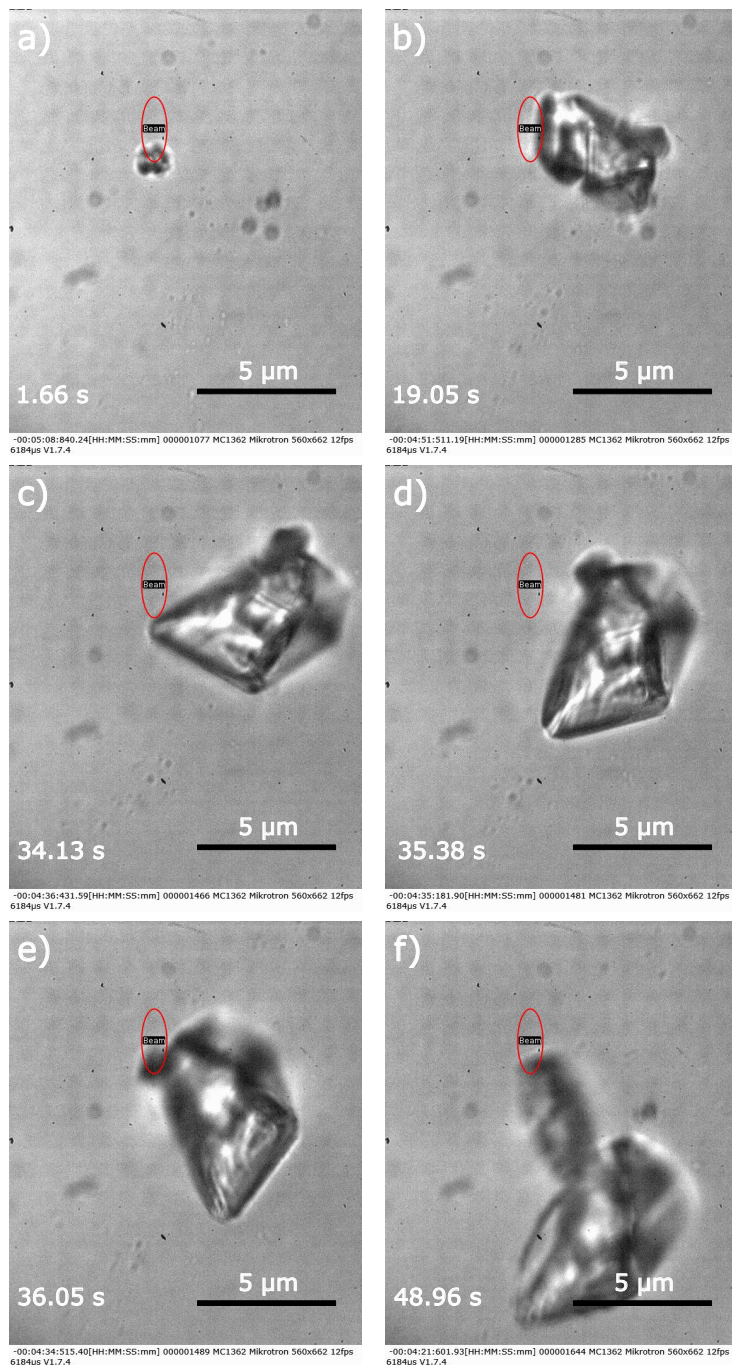


Figure 3.9: Laser induced nucleation at the edge of a droplet of supersaturated glycine solution. (b) shows the first instance of a crystal nucleus, growing quickly through (c)-(e) until after 6.665 s the crystal begins to escape the trap.

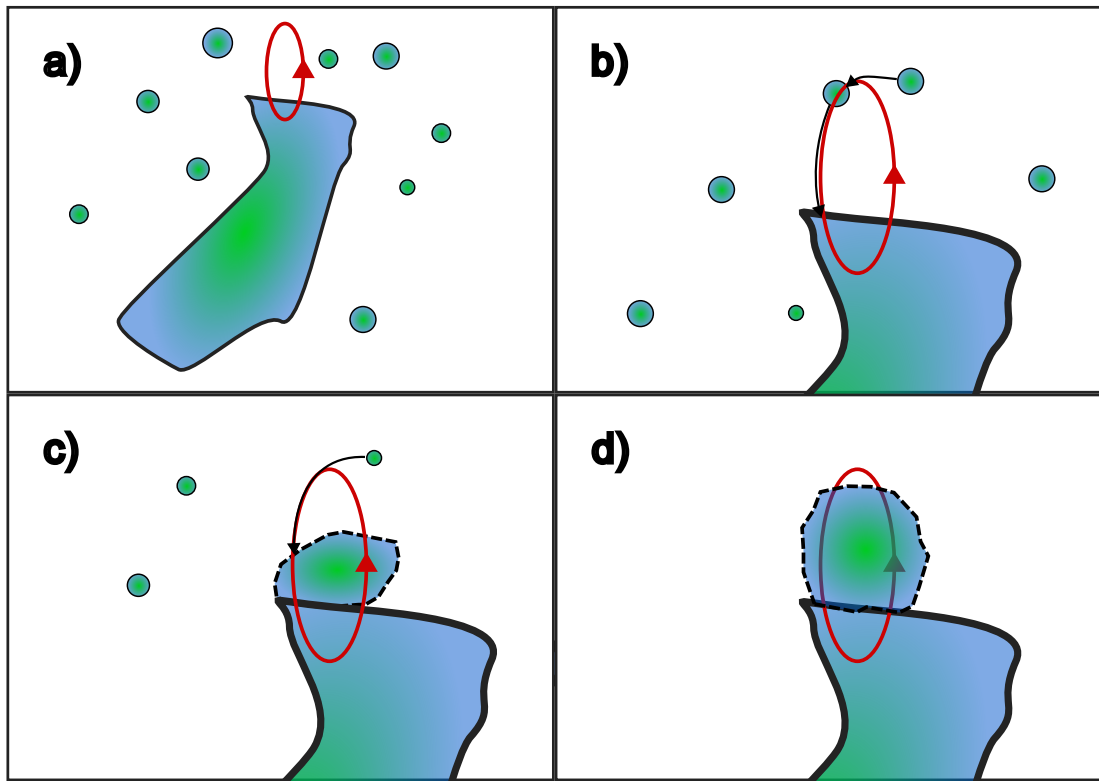


Figure 3.10: Diagram outlining how a moving beam assists in the growth of a crystal nucleus. (a) a crystal nucleus is partially trapped by a moving beam with solute droplets close to its surface. (b) droplets close to the laser focus are drawn in by gradient forces and moved towards the crystal surface. (c) these droplets provide material to the main crystal, resulting in localised growth around the laser focus. (d) eventually the crystal area either fully surrounds the laser focus or the solution surrounding the laser is depleted of solute material.

There are still several factors that need to be investigated, but due to time constraints it was not possible to properly study this phenomena. Firstly, there is the question of what conditions result in the production of concentrated droplets, it is not clear if the presence of a laser is required or if these droplets naturally occurring. Prior literature would suggest that the laser is required [14, 25], but this would not explain why in many cases the droplets are found far outside the influence of the optical trap. It has been suggested that optical traps can attract microspheres over a wider area, but it is hard to say that this would result in the creation of liquid droplets [27].

### 3.9 Conclusion

# Bibliography

- [1] Y. Arita, J. M. Richards, M. Mazilu, G. C. Spalding, S. E. Skelton Spesyvtseva, D. Craig, and K. Dholakia. Rotational dynamics and heating of trapped nanovaterite particles. *ACS Nano*, 10(12):11505–11510, Dec. 2016.
- [2] K. Berg-Sørensen and H. Flyvbjerg. Power spectrum analysis for optical tweezers. *Nature*, 75:594–612, 2004.
- [3] A. I. Bishop, T. A. Nieminen, N. R. Heckenberg, and H. Rubinsztein-Dunlop. Optical microrheology using rotating laser-trapped particles. *Physical Review Letters*, 92(19):198104, May 2004.
- [4] U. G. Būtaitė, G. M. Gibson, Y.-L. D. Ho, M. Taverne, J. M. Taylor, and D. B. Phillips. Indirect optical trapping using light driven micro-rotors for reconfigurable hydrodynamic manipulation. *Nature Communications*, 10(1), Mar. 2019.
- [5] R. Debuyschère, B. Rimez, A. Zaccone, and B. Scheid. Experimental and theoretical investigation of nonclassical shear-induced nucleation mechanism for small molecule. *Crystal Growth & Design*, 23(7):4979–4989, June 2023.
- [6] J. Flannigan. *Optical tweezer and particle control of nucleation and growth at the microscale*. PhD thesis, University of Strathclyde, 2023.
- [7] B. A. Garetz, J. E. Aber, N. L. Goddard, R. G. Young, and A. S. Myerson. Non-photochemical, polarization-dependent, laser-induced nucleation in supersaturated aqueous urea solutions. *Physical Review Letters*, 77(16):3475–3476, Oct. 1996.

## Bibliography

- [8] B. A. Garetz, J. Matic, and A. S. Myerson. Polarization switching of crystal structure in the nonphotochemical light-induced nucleation of supersaturated aqueous glycine solutions. *Physical Review Letters*, 89(17):175501, Oct. 2002.
- [9] G. M. Gibson, J. Leach, S. Keen, A. J. Wright, and M. J. Padgett. Measuring the accuracy of particle position and force in optical tweezers using high-speed video microscopy. *Optics Express*, 16(19):14561, Sept. 2008.
- [10] O. Y. Gowayed, T. Moosa, A. M. Moratos, T. Hua, S. Arnold, and B. A. Garetz. Dynamic light scattering study of a laser-induced phase-separated droplet of aqueous glycine. 125:7828–7839, 2021.
- [11] H.-I. Kim, I.-J. Joo, S.-H. Song, P.-S. Kim, K.-B. Im, and C.-H. Oh. Dependence of the optical trapping efficiency on the ratio of the beam radius-to-the aperture radius. *Journal of the Korean Physical Society*, 43(3):348, 2003.
- [12] G. Knöner, S. Parkin, N. R. Heckenberg, and H. Rubinsztein-Dunlop. Characterization of optically driven fluid stress fields with optical tweezers. *Physical Review E*, 72(3):031507, Sept. 2005.
- [13] D. Konopacka-Łyskawa. Synthesis methods and favorable conditions for spherical vaterite precipitation: A review. *Crystals*, 9(4):223, Apr. 2019.
- [14] Z. Liao and K. Wynne. A metastable amorphous intermediate is responsible for laser-induced nucleation of glycine. 144:6727–6733, 2022.
- [15] J. Millen, T. Deesawan, P. Barker, and J. Anders. Nanoscale temperature measurements using non-equilibrium brownian dynamics of a levitated nanosphere. *Nature Nanotechnology*, 9(6):425–429, May 2014.
- [16] F. Mura and A. Zaccone. Effects of shear flow on phase nucleation and crystallization. *Physical Review E*, 93(4):042803, Apr. 2016.
- [17] S. J. Parkin, R. Vogel, M. Persson, M. Funk, V. L. Loke, T. A. Nieminen, N. R. Heckenberg, and H. Rubinsztein-Dunlop. Highly birefringent vaterite microspheres:

## Bibliography

- production, characterization and applications for optical micromanipulation. *Optics Express*, 17(24):21944, Nov. 2009.
- [18] S. N. S. Reihani, M. A. Charsooghi, H. R. Khalesifard, and R. Golestanian. Efficient in-depth trapping with an oil-immersion objective lens. 31:766, 2006.
- [19] R. M. Robertson-Anderson. Optical tweezers microrheology: From the basics to advanced techniques and applications. *ACS Macro Letters*, 7(8):968–975, Aug. 2018.
- [20] P. Rodríguez-Sevilla, Y. Arita, X. Liu, D. Jaque, and K. Dholakia. The temperature of an optically trapped, rotating microparticle. *ACS Photonics*, 5(9):3772–3778, Aug. 2018.
- [21] T. Rungsimanon, K. ichi Yuyama, T. Sugiyama, and H. Masuhara. Crystallization in unsaturated glycine/d<sub>2</sub>o solution achieved by irradiating a focused continuous wave near infrared laser. 10:4686–4688, 2010.
- [22] K. Saito and Y. Kimura. Optically driven liquid crystal droplet rotator. *Scientific Reports*, 12(1), Oct. 2022.
- [23] T. Sugiyama, T. Adachi, and H. Masuhara. Crystal growth of glycine controlled by a focused cw near-infrared laser beam. *Chemistry Letters*, 38(5):482–483, Apr. 2009.
- [24] T. Sugiyama and S.-F. Wang. Manipulation of nucleation and polymorphism by laser irradiation. *Journal of Photochemistry and Photobiology C: Photochemistry Reviews*, 52:100530, Sept. 2022.
- [25] Y. Tsuboi, T. Shoji, and N. Kitamura. Optical trapping of amino acids in aqueous solutions. *The Journal of Physical Chemistry C*, 114(12):5589–5593, Dec. 2009.
- [26] G. Volpe, O. M. Maragò, H. Rubinsztein-Dunlop, G. Pesce, A. B. Stilgoe, G. Volpe, G. Tkachenko, V. G. Truong, S. N. Chormaic, F. Kalantarifard, P. Elahi, M. Käll, A. Callegari, M. I. Marqués, A. A. R. Neves, W. L. Moreira, A. Fontes, C. L.

## Bibliography

- Cesar, R. Saija, A. Saidi, P. Beck, J. S. Eismann, P. Banzer, T. F. D. Fernandes, F. Pedaci, W. P. Bowen, R. Vaippully, M. Lokesh, B. Roy, G. Thalhammer-Thurner, M. Ritsch-Marte, L. P. García, A. V. Arzola, I. P. Castillo, A. Argun, T. M. Muenker, B. E. Vos, T. Betz, I. Cristiani, P. Minzioni, P. J. Reece, F. Wang, D. McGloin, J. C. Ndukaife, R. Quidant, R. P. Roberts, C. Laplane, T. Volz, R. Gordon, D. Hanstorp, J. T. Marmolejo, G. D. Bruce, K. Dholakia, T. Li, O. Brzobohatý, S. H. Simpson, P. Zemánek, F. Ritort, Y. Roichman, V. Bobkova, R. Wittkowski, C. Denz, G. V. P. Kumar, A. Foti, M. G. Donato, P. G. Gucciardi, L. Gardini, G. Bianchi, A. V. Kashchuk, M. Capitanio, L. Paterson, P. H. Jones, K. Berg-Sørensen, Y. F. Barooji, L. B. Oddershede, P. Pouladian, D. Preece, C. B. Adiels, A. C. De Luca, A. Magazzù, D. Bronte Ciriza, M. A. Iati, and G. A. Swartzlander. Roadmap for optical tweezers. *Journal of Physics: Photonics*, 5(2):022501, Apr. 2023.
- [27] P.-W. Yi, W.-H. Chiu, T. Kudo, T. Sugiyama, R. Bresolí-Obach, J. Hofkens, E. Chatani, R. Yasukuni, Y. Hosokawa, S. Toyouchi, and H. Masuhara. Cooperative optical trapping of polystyrene microparticle and protein forming a submillimeter linear assembly of microparticle. *The Journal of Physical Chemistry C*, 125(34):18988–18999, Aug. 2021.
- [28] Yogesha, S. Bhattacharya, and S. Ananthamurthy. Characterizing the rotation of non symmetric objects in an optical tweezer. *Optics Communications*, 285(10–11):2530–2535, May 2012.
- [29] K.-i. Yuyama, T. Rungsimanon, T. Sugiyama, and H. Masuhara. Formation, dissolution, and transfer dynamics of a millimeter-scale thin liquid droplet in glycine solution by laser trapping. *The Journal of Physical Chemistry C*, 116(12):6809–6816, Mar. 2012.
- [30] K.-i. Yuyama, T. Sugiyama, and H. Masuhara. Millimeter-scale dense liquid droplet formation and crystallization in glycine solution induced by photon pressure. *The Journal of Physical Chemistry Letters*, 1(9):1321–1325, Apr. 2010.